Study of bubble's equilibrium in rotating flow

Marie Rastello, Jean-Louis Marié, Nathalie Grosjean, Michel Lance

6th International Conference on Multiphase Flow,
ICMF 2007, Leipzig, Germany, July 9 – 13, 2007

Study of bubble's equilibrium in rotating flow

Marie Rastello, Jean-Louis Marié, Nathalie Grosjean and Michel Lance

Laboratoire de Mécanique des Fluides et d'Acoustique, UMR CNRS 5509,

Ecole Centrale de Lyon/Université Claude Bernard Lyon 1/INSA Lyon

LMFA - ECL, 36 avenue Guy de Collongue, 69134 Ecully cedex, France

marie.rastello@ec-lyon.fr, jean-louis.marie@ec-lyon.fr, nathalie.grosjean@ec-lyon.fr, michel.lance@ec-lyon.fr

Keywords: bubble, lift force, drag force, wake interaction, rotating flow

Abstract

The equilibrium of small bubbles ($d \in [0.2\,\mathrm{mm}, 2\,\mathrm{mm}]$) in a solid body rotating flow around an horizontal axis is studied. The caracterisation of the reference flow (eg) the rotating flow without bubbles is led. Measurements show that the velocity profiles are linear as expected and that the axis of rotation of the flow exhibits motions of small amplitude ($\approx \pm 0.1\,\mathrm{mm}$). The frequencies that appear in this motion are explored. One peak is the rotation rate of the tank, frequency that is also present in the bubble's oscillating motion. The influence of the bubbles on this reference flow is then investigated. Depending of the size of the bubble and of its position relatively to the axis of rotation the bubble can feel back its own perturbation. The range of Reynolds and Strouhal numbers in which this occurs is quantified. When the incoming flow on the bubble is not influenced by the wake of the bubble, the drag and lift coefficients are considered. The two coefficients are determined from the measurement of the bubble's equilibrium position. The resulting coefficients exhibit an increase of the drag with shear and a decrease of the lift. The lift coefficient tends asymptotically to 1 at high Reynolds number which is higher than the 0.5 value of Auton (1987)'s potential theory. The bubble never stabilizes on its equilibrium position, but slightly oscillates around this position. The spectrum of these oscillations shows three types of frequencies. One is equal to the rotation rate of the tank, another one is linked with a three-dimensional motion of the bubble and the last one is related to the interaction between the bubble and the shedding of vortices in the wake.

1 Introduction

In many industrial processes such as oil industry or chemical engineering for example, it is essential to know, as far as possible, the motion of bubbles relatively to the fluid to be able to predict the dynamic of the whole flow or the efficiency of the chemical reaction. To that purpose, it is necessary to understand the forces acting on each bubble and to have an expression or a value of them in the considered context. Referring to recent simulations, a calculation of the forces becomes now possible (see for example Lu *et al.* (2006)). Nevertheless, to increase the number of bubbles that can be simulated, reliable information on theses forces is required. From several aspects such as deformable versus rigid shape or zero-stress versus non-zero stress condition at the interface, bubbles differ from particles. The forces cannot then be simply deduced from the one applied on particles. At present even the forces on a single bubble are under discussion and their expression is not unanimously established. When the flow is sheared or the bubble deformed a key problem lies in the lift force (Magnaudet & Eames 2000). Analytical developments exist in different asymptotic cases. The viscous case has been considered by Saffman (1965) for a small rigid sphere in a linear shear flow with large shear. The analysis was extended by McLaughlin (1991) taking into account inertia effects. Legendre & Magnaudet (1997) revisited Saffman results and obtained a lift force $(2/3)^2$ that of a solid sphere. The other limit, that of inviscid fluids, was explored, among others, by Auton (1983, 1987). In the case of a weak linear shear flow, the lift coefficient value obtained is 0.5. Numerical studies have been performed to determine the forces in generic flow situations such as uniform or linear shear flows (Legendre & Magnaudet 1998) and predictive laws have been determined for the drag and lift forces depending on the Reynolds number and on the shear rate. Simultaneously, experiments were performed following the same kind of ideas: reference flows were studied such as to have reference values for the forces and especially the lift force. Naciri (1992) studied the equilibrium position of a bubble in a solid body rotating flow around an horizontal axis and deduced from it values and some scaling for the lift and drag forces. The fluids were water and glycerin/water mixtures, the bubbles were seemingly of the order of a few millimeters. In parallel to the present study another one still on the same kind of flow has been performed with water and glycerin/water mixtures with millimetric bubbles (Van Nierop 2003; Van Nierop *et al.* 2007). Results on both drag and lift forces have been obtained, especially a change of sign of the lift force when the Reynolds number becomes low has been observed. The present study

also concerns a solid body rotating flow around an horizontal axis. It concentrates on moderate to high Reynolds numbers with low to moderate values of the shear rate. The forces are determined and the effect of Reynolds and shear are studied. Attention is payed to occurring phenomena that can disturb this measurement. In particular, the interaction between the bubble, its wake and the reference flow and on the conditions for which the interaction occurs is studied. A particular feature is that the bubble never stabilizes completely, it is always moving, oscillating around its equilibrium position. The movements are of small amplitude (a few tenths of a millimeter) but with specified frequencies. Some work also concerns this aspect. The outline of the paper is as follows. Section 2 presents the force balance for a bubble, and how in the framework of a horizontal solid body rotation the measurement of the equilibrium position gives access directly to the forces applied to the bubble. The experimental setup, the caracterisation of the reference flow and the measurement process are presented in section 3. The measured drag and lift forces come with section 4. The last part deals with the oscillating motions of the bubble.

2 Force balance on a bubble.

In the present section, the force balance on a bubble is given and then applied for the bubble at its equilibrium position in the solid body rotating flow. Some non-dimensional numbers that can be used to describe the system are then presented. For a clean, uncontaminated, spherical bubble, moving relatively to the fluid at moderate to large Reynolds number, the dynamical equation is (Magnaudet & Eames 2000):

$$\rho_l V_b C_A \frac{d\mathbf{v}}{dt} = -\rho_l V_b \mathbf{g} + \rho_l V_b (C_A + 1)\frac{D\mathbf{U}}{Dt} \qquad (1)$$
$$+\rho_l V_b C_L (\mathbf{U}-\mathbf{v}) \times (\nabla \times \mathbf{U}) + \frac{1}{2}\rho_l C_D A_b |\mathbf{U}-\mathbf{v}|(\mathbf{U}-\mathbf{v})$$

where ρ_l is the liquid density, V_b the volume of the bubble, A_b its projected area, $\mathbf{v}$ the bubble velocity, $\mathbf{g}$ the acceleration due to gravity and $\mathbf{U}$ the velocity of the undisturbed ambient flow taken at the center of the bubble. The gas density is neglected because $\rho_g \ll \rho_l$. C_A is the added mass coefficient, its value is 0.5 for spherical bubbles (Magnaudet & Eames 2000) and depends on the ratio between the major and the minor axis for ellipsoidal ones (Lamb 1934). C_L is the lift coefficient and C_D the drag coefficient. Because the bubble is a sphere the lift here is only induced by shear and not by bubble deformation.

The present study deals with a bubble immersed in a fluid in solid-body rotation around an horizontal axis. As mentioned before a first positive point for the present study is that the bubble is immersed in a reference flow. Another major interest of the setup is that the bubble comes roughly to an equilibrium position in the non-transient regime. This gives the opportunity to measure the forces without having to measure an instantaneous velocity or acceleration for the bubble. Mentioned in the order of appearance in equation (1), the forces applied on the bubble are F_B the buoyancy force, F_A which takes into account the added mass force and pressure gradient effects, F_L the lift force and F_D the drag force (see figure 1). Because $\mathbf{U} = \omega r \mathbf{e}_\theta$, equation (1) at equilibrium can be rewritten in:

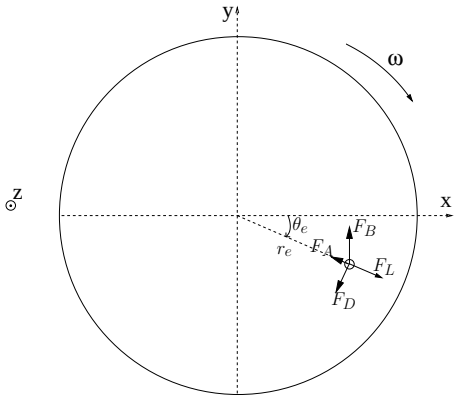

Figure 1: The forces applied on a bubble at equilibrium at moderate to high Reynolds numbers. F_B is the buoyancy force, F_D, the drag force, F_L the lift force. F_A takes into account the added mass force and pressure gradient effects. In the present sketch, the angular velocity ω and equilibrium angle θ_e are negative.

$$C_L = \frac{1}{2}\left(1 + C_A - \frac{g\sin\theta_e}{r_e\omega^2}\right) \qquad (2)$$

and

$$C_D = -\frac{4}{3}\frac{gd\cos\theta_e}{|r_e\omega|r_e\omega} \qquad (3)$$

with ω the angular velocity of the rotating tank and of the fluid, $(r,\ \theta)$ the polar coordinates whose values at equilibrium are $(r_e,\ \theta_e)$ and d the diameter of the bubble. Thus, the measurement of r_e and θ_e when the bubble is at equilibrium, knowing the other characteristics $(d,\ \omega,\ C_A)$ provides a value for the lift and drag coefficients in the non-transient regime.

To describe this non-transient state, the only parameters that are needed are, the angular velocity ω, the diameter of the bubble d, the viscosity ν of the fluid, its density ρ_l and its surface tension σ , all *chosen* by the experimenter and r_e and θ_e measured when the bubble is at equilibrium. These seven parameters need three units. Using the Π-theorem it appears that four non-dimensional parameters are needed to describe the forces applied on the bubble at equilibrium. One possible set is for example the Reynolds number (Re) based on the relative velocity between the bubble (zero) and the fluid (ωr), the Froude number (Fr) which is the ratio between inertia effects and buoyancy, the Strouhal number (Sr) which is a ratio between the difference of velocity seen by both sides of the bubble and the mean velocity of the fluid at the place of the bubble and the Morton number (Mo) which is representative of the characteristics of the fluid:

$$Re = \frac{|\mathbf{v}-\mathbf{U}|d}{\nu},\ Fr = \frac{|\mathbf{v}-\mathbf{U}|^2}{gd},\ Sr = \frac{|\Delta\mathbf{U}|}{|\mathbf{v}-\mathbf{U}|},$$
$$Mo = \frac{g\nu^4\rho^3}{\sigma^3} \qquad (4)$$

Here, the different numbers express as follows:

$$Re = \frac{\omega r_e d}{\nu},\ Fr = \frac{\omega^2 r_e^2}{gd}, Sr = \frac{d}{r_e},\ Mo = \frac{g\nu^4\rho^3}{\sigma^3} \qquad (5)$$

3 The experimental and measuring facilities

This part deals with the presentation of the experiment. First the experimental setup is described. The caracterisation of the reference flow comes after. The part ends with the description of the measuring protocol.

3.1 The experimental setup

The device is made of a Plexiglas cylindrical tank (Ø=10 cm, L=10 cm) rotating around its axis (horizontal). The tank is

Figure 2: Photography of the experimental device showing the tank. In front of it is the high-speed camera. In the back the toothed belt and the opto-electronic sensor can be seen.

mounted in a cylindrical counterbore and the contact is made using ball bearings (see figure 2). A motor is coupled to the tank, at the back, using a toothed belt. The rotation rates for the tank ranges from $1\,\mathrm{rad.s^{-1}}$ to $100\,\mathrm{rad.s^{-1}}$. The motor is driven using a Labview program on the computer. The same program is also used to determine an effective rotation rate of the tank. Indeed, a reflecting sticker has been put on the side of the tank. An opto-electronic sensor detects the passages of the sticker in front of him, the electrical signal is transmitted to the computer. A detection of the rising fronts in the signal is then used to obtain the rotation rate of the tank. The front face of the tank is removable for cleaning use and three aligned holes have been done on the side of the cylinder. They are closed with stoppers. They are used to fill in the tank with water and to inject the bubble.

3.2 Description of the reference flow

Because the purpose of the work is to determine the forces applied on a bubble in a given flow (the solid-body rotating flow), a first step is to check that the flow is effectively the one waited for. Hence, the present part deals with three different aspects of this verification. First, velocity profiles have been determined on the whole section of the tank to check that the flow is effectively a solid body rotation. The second one deals with the position of the axis of rotation of the flow. The purpose was there to see if the axis of rotation of the flow is stable or moving. The last one deals with the study of the flow in presence of a bubble to see if a coupling could appear between the flow and the bubble. Such a coupling could modify the behavior of the bubble and thus the force measurements.

PIV measurements were performed to determine the velocity profiles in the reference flow. Experiments were done with the tank full of water, without any bubble. Small hollow glass spheres of $10\,\mu\mathrm{m}$ diameter (Dantec product) were dispersed in the fluid. The laser sheet was generated perpendicularly to the axis of rotation by a dual-cavity pulsed laser Nd-Yag Quantel $120\,\mathrm{mJ} - 8Hz$. The images were recorded with a low speed camera Dantec FlowSense working at 15 frames per second, using a field of view covering the whole section of the flow (size of the field: $11\,\mathrm{cm}^2$). The measured velocity profiles are all well linear. An example of such a velocity profile is presented on figure (3). The PIV measure-

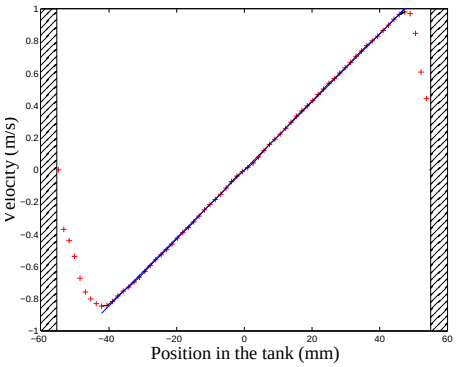

Figure 3: An example of the velocity profiles obtained with the PIV measurements. Here, the velocity of the tank is $1.2\,\mathrm{m/s}$

.

ment was not able to resolve the flow close to the side of the tank. Hence the values obtained on the sides (see figure (3)) are false. To get the true velocity of the fluid near the tank, it is thus necessary to do an extrapolation of the data using a linear regression. As expected, the extrapoled velocity fits well with the velocity of the tank.

To study the possible movements of the axis of rotation of the flow, a second different PIV campaign was done. Indeed, when the experiments are performed with bubbles, bubbles never stabilize completely and always oscillate with one frequency among others that is the rotation frequency of the tank (see section 5). The purpose was then to check if there was or not a precession of the axis of rotation of the fluid, which could make the bubble oscillate. The PIV measurements were done using a reduced field. The field size is $2\,\mathrm{mm}^2$. The particles were fluorescent polyamide spheres doped in Rhodamin B of size $10\,\mu\mathrm{m}$ (Dantec product). They absorbe in the green light and emit in the orange. The laser sheet was perpendicular to the axis of rotation as before. The laser was a Spectra Physics Millenia IIs continuous diode pumped (2W). The camera was a high-speed video camera (Phantom V4.3 black and white) with an orange filter mounted on it. The frame rate used was 200 frames per second. To reduce the field of view to the expected size an Optem Zoom 125C objective was used. For the PIV correlations to be possible in the $2\,\mathrm{mm}^2$ field, a high concentration of seeding particles was necessary. These particles being expensive, the experiment was repeated only four times. The rotation speed of the tank was the same for the four runs. A small motion of the axis of rotation of the flow with a privileged vertical di-

rection is observed (see figure 4). The order of magnitude

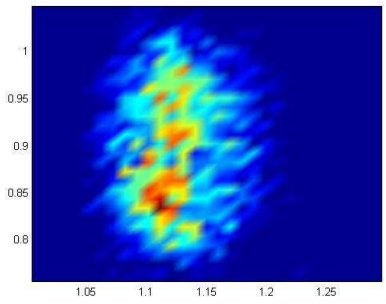

Figure 4: Colored 2d histogramm of the position of the axis of rotation of the flow for a run of 2000 images.

of the amplitude of the motion is about $\pm 0.1\,\mathrm{mm}$. This will be taken into account in the calculation of the uncertainties when studying the bubble's behavior. When looking at the fourier transform of the x-position of the axis of rotation, for the four runs, a peak appears in the spectrum at the rotation rate of the tank. This result is interesting to be connected with the oscillations of the bubble presented in section 5.

The third study of flow behavior was performed with one bubble present in the tank. The purpose was there to investigate if sometimes the bubble can perturb the flow so much that it feels back its own perturbation. In that case, this feedback of the perturbation makes the incoming flow on the bubble to be also modified. It is important to be able to discriminate these "perturbed" cases from the "unperturbed" ones while working on the values of the forces (see section 4). The study was done using PIV measurements in the flow surrounding the bubble to see where and when perturbations appear. A global view of the perturbed zone was sought. PIV measurements were here again performed with the fluorescent particles, the continuous laser and the high speed camera with the orange filter but with a standard objective (60 mm) and a frame rate of 900 images per second. The procedure is the following. PIV measurements were successively performed with the bubble stabilized in the laser sheet and without the bubble, keeping the same rotation rate. Then, the velocity field obtained from the run without bubble and averaged on the 2000 fields was substracted to the instantaneous fields with the bubble. This gives access to the way the bubble disturbs the basic solid rotation velocity field. Then, using a sliding averaging operation, the disturbed fields are averaged over 50 instantaneous fields. The obtained disturbed averaged fields are then visualized to see when the wake of the bubble modifies so much the reference flow that it feels it back. Examples are presented on figures (5), (6) and (7). Figure (5) presents an example of the resulting fields obtained for a small bubble ($d \approx 0.5\,\mathrm{mm}$, $Re \approx 20$). For this kind of bubbles, whatever the position of the bubble in the tank and thus whatever the Strouhal number the wake is so small that it does not perturb significantly the flow. Indeed, when looking at the 2000 disturbed averaged fields for such small bubbles, the center of the tank, here around $X = 8.5\,\mathrm{mm}$, $Y = -0.5\,\mathrm{mm}$, always presents velocity vectors that are practically zero. Figure (6) and (7)

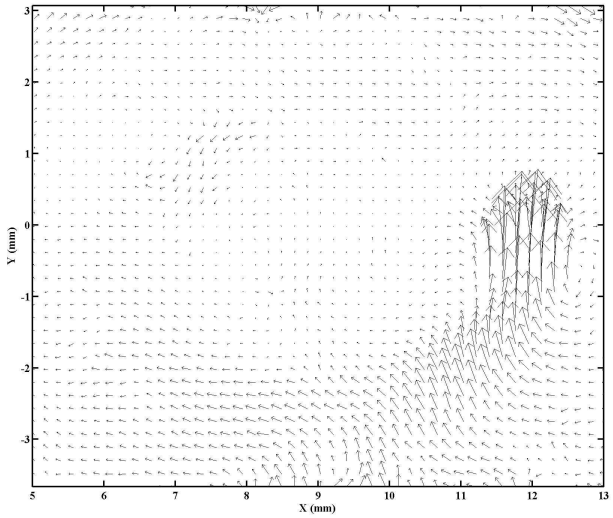

Figure 5: A small bubble ($d \approx 0.5\,\mathrm{mm}$, $Re \approx 20$) and its wake. The center of the tank is around $X = 8.5\,\mathrm{mm}$, $Y = -0.5\,\mathrm{mm}$. The field is obtained using a sliding average over 50 instantaneous fields to which the basic solid rotation field has been substracted. The bubble is located where the large vectors are. The center of the flow appears as not perturbed by the presence of the bubble. In this case $Sr^{-1} \approx 6 - 7$.

deal with middle size bubbles ($d \approx 0.9\,\mathrm{mm}$, $Re \approx 80$ for figure (6) and $d \approx 1\,\mathrm{mm}$, $Re \approx 100$ for figure (7)). For this kind of bubbles, three behaviors have been pointed out. First for large Strouhal numbers (eg) small distances to the center relatively to the diameter the wake perturbs the center of the reference flow and the bubble feels this perturbation. A coupling between the bubble and the reference flow arises and the system becomes different from the one that should be studied. This concerns $Sr^{-1} \lesssim 6$. Figure (6) is an illustration of such a behavior. The two images are two disturbed averaged fields for the same bubble during a run. The center of the tank is around $X = 13.5\,\mathrm{mm}$, $Y = -0.5\,\mathrm{mm}$. The comparison of both images show that when the bubble and its wake oscillate they induce fluid aspirations and forcings back in the zone of the center of the tank; zone that is close to the bubble. For $6 \lesssim Sr^{-1} \lesssim 10$ and the same kind of bubbles, an example is on figure (7). What can be observed is that even long and oscillating with the bubble, the wake of the bubble only induces very low secondary flows toward the center of the tank ($X = 13.5\,\mathrm{mm}$, $Y = 1.5\,\mathrm{mm}$) that seem to have a quasi-negligible back influence on the bubble. Thus, in this range the wake perturbs a little bit the center of the flow but it seems that the perturbation is very weak. However, at the present stage it is difficult to tell if such a weak perturbation still has a small influence on the measured forces or not. For this kind of bubbles the case $10 \lesssim Sr^{-1}$ (bubbles far from the center) exhibits no coupling and no perturbation coming back onto the bubble. The incoming flow onto the bubble is a clean flow of solid body rotation. When the size of the bubble increases ($Re \gtrsim 100$), the three regions for the Strouhal number remain. In that case the perturbation of the center, when present is even stronger and a very large coupling can appear for $Sr \lesssim 6$. An example of such a coupling

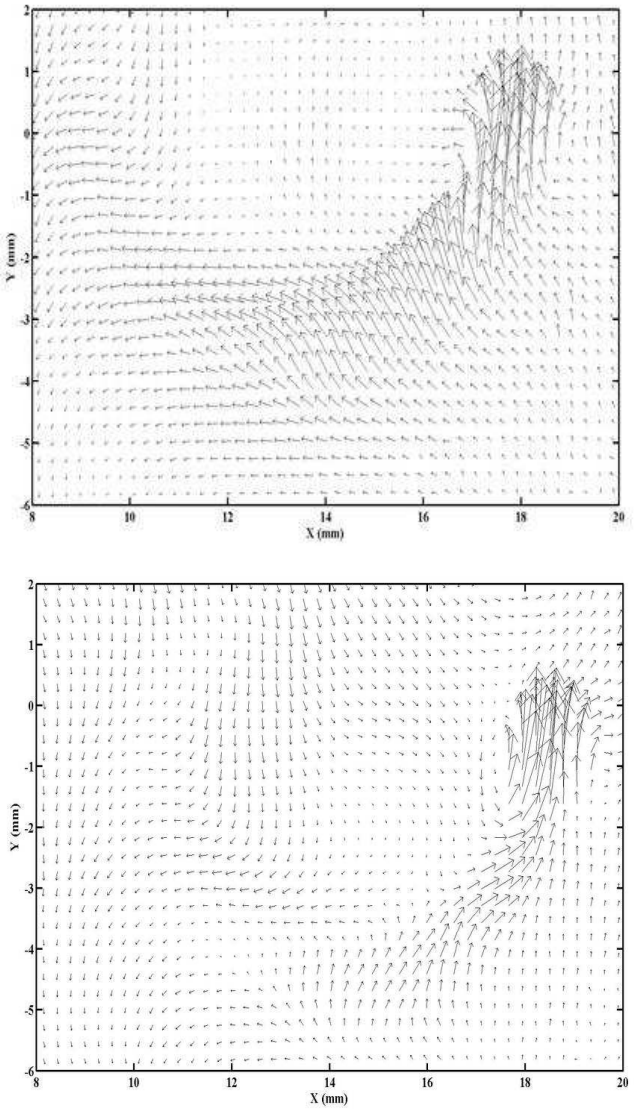

Figure 6: A middle size bubble ($d \approx 0.9\,\mathrm{mm}$, $Re \approx 80$) and its wake at two different instants. The center of the tank is around $X = 13.5\,\mathrm{mm}$, $Y = -0.5\,\mathrm{mm}$. The field is obtained using a sliding average over 50 instantaneous fields to which the basic solid rotation field has been substracted. The bubble is located where the large vectors are. Comparing the two images it can be observed that the bubble's wake perturbs the center of the flow. The bubble feels that perturbation and its motion and behavior are modified. In this case $Sr^{-1} \approx 5$

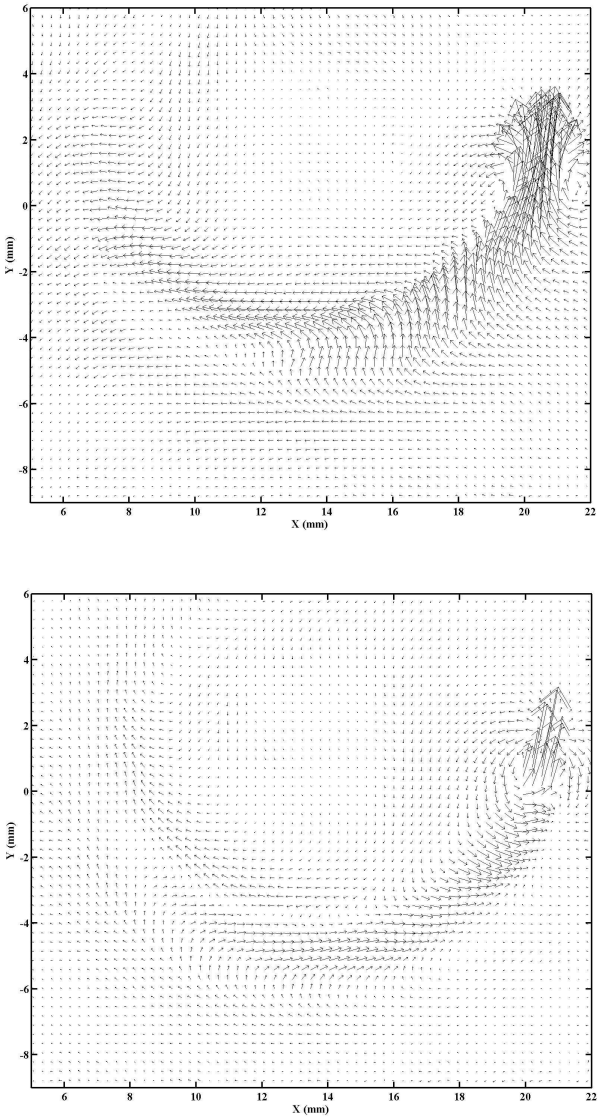

Figure 7: A middle size bubble ($d \approx 1\,\mathrm{mm}$, $Re \approx 100$) and its wake, at two different instants. The center of the tank is around $X = 13.5\,\mathrm{mm}$, $Y = 1.5\,\mathrm{mm}$. The field is obtained using a sliding average over 50 instantaneous fields to which the basic solid rotation field has been substracted. The bubble is located where the large vectors are. Comparing the two images it can be observed that the wake has only a very small influence on the center of the flow. The bubble in this case seems not to feel that perturbation. $Sr^{-1} \approx 7$

is shown on figure (8). The images were done with a long

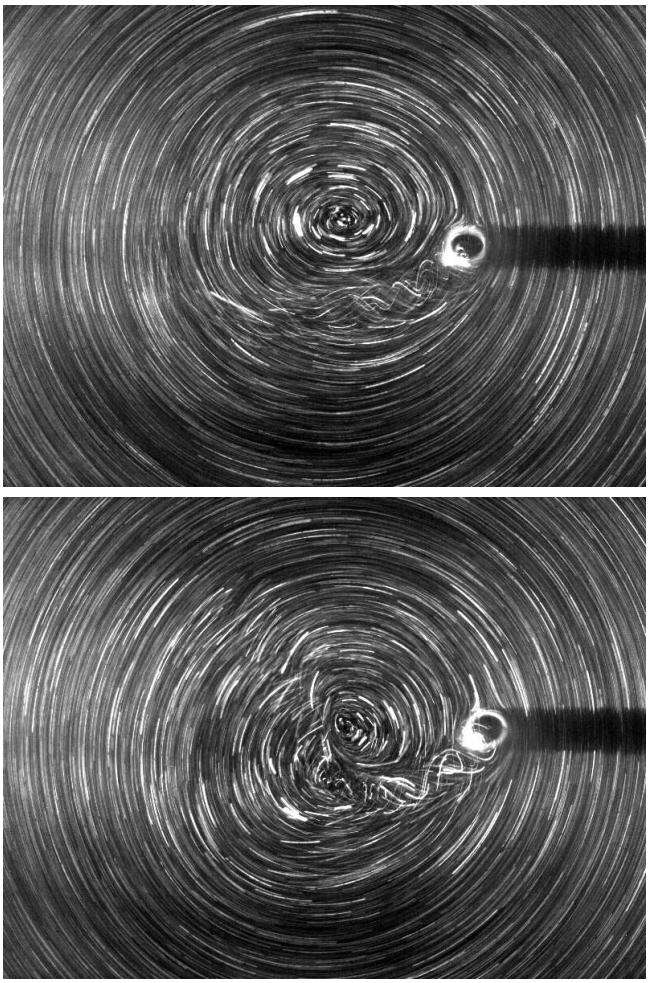

Figure 8: Long time exposure for a "large" bubble. In that case, $Re > 100$, $Sr^{-1} < 6$ and a strong coupling between the bubble and its perturbation occurs.

time exposure for the camera. During a run, depending on the moment, one, two or three vortices can appear in the region of the center (see for example right side of figure (8)). These vortices directly interact with the bubble. Nevertheless, as for smaller bubbles, for larger values of Sr^{-1}, the bubble here again doesn't feel any feedback of its perturbation. All these behaviors can be classified as follows. For bubbles with $Re \lesssim 60 - 70$, whatever the position of the bubble in the tank and thus the Strouhal number it does not feel its own perturbation. That is due to the smallness of the wake. For larger Reynolds numbers, when $Sr^{-1} \lesssim 6$, there is a clear coupling between the bubble and its own perturbation. The incoming flow on the bubble is no more a pure flow of solid body rotation. For $6 \lesssim Sr^{-1} \lesssim 10$, a slight influence of the perturbated zone on the bubble may occur and for $10 \lesssim Sr^{-1}$ no perturbation is felt back by the bubble.

3.3 Description of the experiment with a bubble

The experiments are performed as follows. The tank is filled with demineralized water. When all the residual bubbles have been removed, a unique bubble is injected. The range of sizes of the bubbles is $[0.2\,\mathrm{mm}; 2\,\mathrm{mm}]$. After the injection has been performed, the tank is set in rotation. It is then necessary to wait for a few minutes for the flow and the bubble to reach their non-transient regime. Non-transient regime means for the fluid to be in solid body rotation. For the bubble it means to have reached its equilibrium position. In practice the bubble never stabilizes completely. It oscillates around the equilibrium position even after a long time waiting. Nevertheless, the amplitudes are small. The order of magnitude is a few tenths of a millimeter.

When the bubble has reached its non-transient regime and oscillates around its equilibrium position, the measurements begin. The position of the bubble in the direction parallel to the axis of rotation Z is determined, using a laser pointer moving along a rod located above the tank. In practice, the laser beam is changed into a sheet using a small cylindrical lens. The laser sheet is oriented to be parallel to the faces of the cylinder. This sheet is translated manually till it intercepts the bubble. This gives the bubble's position Z. The bubble is filmed using the high-speed video camera aligned with the cylinder. Indeed the camera is mounted on a rail and has been very carefully aligned with the cylinder with micrometer screw translating devices. The rail is bound to the structure of the experiment to remain aligned. It is supported by an iron bar covered with rubber and fixed to the wall of the room to reduce vibrations. The frame rate is 100 frames per seconds and the recording lasts around 20 seconds. After a run, the 2000 images are then transferred on the computer and treated using a Matlab software. On each image the position of the bubble (r, θ), its size, its flatness and its applied forces and non-dimensional numbers are determined.

3.4 Characteristics of the measurement

In the present section, the difficulties inherent to the measurement are presented. It is followed by the description of the way the bubble characteristics are determined. The main difficulty with the present experiment is that the stabilization point of the bubbles is very close to the horizontal axis and then $\sin\theta$ and θ are very small. Indeed, θ is of the order of a few radians. Thus, the measurement of θ requires a lot of precision. The three principal sources of uncertainty in the measurement of the parameters have been inventoried and quantified.

The first difficulty is to convert the pixels of the image into physical length units for the plane at position Z, where the bubble is stabilized. This is achieved as follows. An image of two circular test patterns, temporarily fixed on the front and back faces of the tank, is captured (see for example figure 9). This provides the ratios between pixels and centimeters for the two faces distant of $10\,\mathrm{cm}$. Using the laser pointer sheet the Z position of the bubble has been determined, with a precision of $\pm 1\,\mathrm{mm}$. The ratio between pixels and centimeters at the location of the bubble is then obtained using a linear regression. The typical order of magnitude of the ratio between centimeters and pixels is: 220 pixels/cm for the front face and 130 pixels/cm for the back face.

The second point that needs attention is that despite all the care used to align the camera a small misalignment can

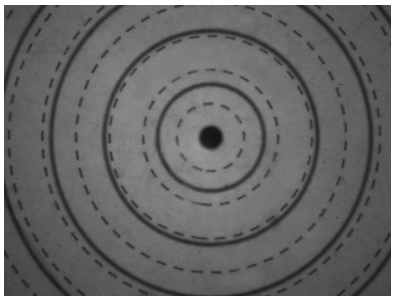

Figure 9: Image of the tank with both circular test patterns put on the faces to determine the ratio between pixels and centimeters. The continuous line is on the test pattern of the front face, the dotted one is the one on the rear face. The space between two successive similar lines corresponds to 0.5 mm.

remain. Its order of magnitude is a few pixels. So small it is, it must be corrected because for the bubbles that have their equilibrium position close to the horizontal axis, it can be of the same order of magnitude as the Δy between the bubble and the horizontal axis. Because it was not possible to be more precise in the alignment it was decided to measure the shift between the axis of the tank and of the camera and to apply a correction to the results. The principle is as follows. First a circular sticker with a diameter of the order of $1\ \mathrm{cm}$ is put on the front face. Its motion is captured when the tank is rotating. The center of the circle described by the center of the sticker is determined. This gives the measured center of the front face. The same protocol is then performed with the back face. This provides a measurement of the shift between both measured centers and thus of the misalignment. As for the ratio between pixels and centimeters a linear regression is then used to determine the effective position of the center of the tank in the plane in which the bubble is stabilized. In the present measurements the typical shift between both centers is of the order of 3 pixels in x and 3 pixels in y. The precision of the measured shift is $\pm 0.25\,\mathrm{pixels}$.

The third and last aspect that need to be payed attention to are the vibrations of the camera. Indeed, even fixed on a rail itself attached to the experiment which is heavy, the camera is sensitive to vibrations of the working environment, such as ground vibrations. These vibrations can cause small instantaneous misalignments of the camera, which are source of noise on the results. This problem was partly removed by calculating the bubble position on each image relative to the instantaneous center of rotation seen by the camera. This center is given by the trajectory of a small sticker glued on the center of the front face of the tank. As the sticker could not be perfectly centered on the rotation axis, it describes each turn a small circle. The center of the circle accomplished during the N/2 images before and the N/2 images after the bubble image treated, N being the number of images for the tank to do a turn, is considered as the instantaneous center of rotation of the front face and used to calculate, after the Z correction, the bubble position. The precision on the determination of the center is estimated as $\pm 1\,\mathrm{pixel}$. During this procedure a fourier transform of the x-position of the center of the sticker is performed. The resulting peak gives the rotation rate of the tank ω with a precision of $\pm 0.15\,\mathrm{rad/s}$. This measurment is more precise than the one obtained with the opto-electronic sensor.

The treatment of the images with the Matlab software to determine the useful characteristics for the bubble is performed as follows. A first pass on all the 2000 images is done to determine the instantaneous positions of the center of the tank with the sliding technique as described before. Then, using the image with the test patterns the ratio pixel versus centimeters is determined for the front and back face. Knowing the position of the bubble in the tank determined with the laser sheet, the ratio is calculated for the bubble position. All the images are then treated a second time to determine the bubble characteristics. A mask is applied around the bubble, then a threshold is determined automatically and applied to the image to detect the bubble. The image is binarized and the size of the bubble, its position and its flatness are determined in pixels and then converted in real size. For all the studied bubbles the flatness is less than 1.1. Knowing the position of the center of the tank for each image, r and θ can be determined. The forces are then calculated using equations (2) and (3). During the image treatment, the uncertainties of the different parameters have been evaluated. d has a precision of $\pm 1\,\mathrm{pixel}$. As for the center of the tank, the precision of the bubble position is $\pm 1\,\mathrm{pixel}$. As a first approximation, this gives an uncertainty for C_L of the order of 30% to 40% and 15% for C_D. Calculating C_D and C_L can be done using the instantaneous values of the parameters and then averaging the coefficient over the 2000 images. It can also be calculated directly with the mean value of the parameters. It was checked that the values of the coefficient are the same to the order of our precision if calculated using the mean value of the parameters or if averaged afterwards.

4 Drag and lift forces

In the present section are presented the results for the drag and lift forces and the comparison to existing results.

4.1 Drag force

As usual, the drag coefficients are plotted as a function of the Reynolds number (see figure 10). The experimental data have been classified into three categories saying $4 \leq Sr^{-1} < 6$ (green stars), $6 \leq Sr^{-1} < 10$ (red x) and $10 \leq Sr^{-1}$ (blue cross). Two curves are also plotted. The upper one is the drag for solid spheres (Clift *et al.* 1978):

$$C_D = \frac{24}{Re}(1 + 0.15Re^{0.687}) \tag{6}$$

The lower one is the one for clean bubbles (Mei *et al.* 1994):

$$C_D = \frac{16}{Re}\left(1 + \left(\frac{8}{Re} + \frac{1}{2}(1 + 3.315Re^{-1/2})\right)^{-1}\right) \tag{7}$$

Both curves have been obtained for bubbles in a uniform flow. As discussed in section 3.2 bubbles with $4 \leq Sr^{-1} < 6$ and $Re \gtrsim 60 - 70$ are so close to the axis of rotation of the flow, that a significant coupling exists between the reference flow, the bubble and its wake. This modifies the incident flow

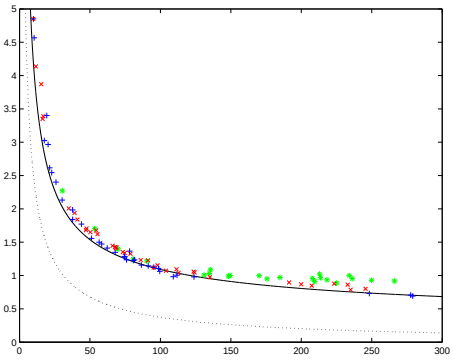

Figure 10: Drag coefficient C_D as a function of Reynolds number Re. + are bubbles with $10 \leq Sr^{-1}$, x are bubbles with $6 \leq Sr^{-1} < 10$, * are bubbles with $4 \leq Sr^{-1} < 6$, the plain line is the drag curve for solid spheres and the dashed line is that of clean bubbles.

arriving on the bubble and in that case the measurements cannot be considered as representative of the drag in a pure rotating flow. They are therefore disregarded. Nevertheless, it is interesting to note that coupling effects increase the drag coefficient. This is particularly visible for $Re > 100$ (green stars). In the range $10 \leq Sr^{-1}$ (blue plus) there is no such two-way coupling and the incident solid rotation flow on the bubbles is not affected. The drag coefficient for these bubbles coincides rather well with the curve for solid spheres. Two main reasons can explain this trend. The first one is that the interface of the bubble is entirely contaminated. Such a possibility cannot be excluded, but is surprising given the care we have brought to work with clean water. We would expect that interfaces be weakly contaminated and the data to fall between the curve for solid sphere and clean bubble. The second reason for the data be higher than the curve for clean bubbles in uniform flow can be the effect of the shear. Indeed, Legendre & Magnaudet (1998) performed numerical simulation in a linear shear flow for moderate to large Reynolds number showing that shear effects increased the drag coefficient, according to a relation in the form

$$C_{Dshear}(Re, Sr) = C_{Duniform} \times (1 + 0.55Sr^2) \qquad (8)$$

A detailed inspection of our experimental points reveals that drag coefficient increases with the shear rate. This clearly appears for $Re \leq 60 - 70$ in the range $6 \leq Sr^{-1} < 10$ (red cross); $4 \leq Sr^{-1} < 6$ (green stars), where there is no two-way coupling (section 3.2) and the points are systematically above the solid drag curve. Interestingly, this increase with the dimensionless shear number Sr seems more pronounced than the increase predicted for the linear shear flow. We tried to fit our points using a relation similar to equation (8) and found a coefficient of the order of 5 instead of 0.55. If we correct the data to account for shear effects as it was done by Van Nierop *et al.* (2007) using this value of 5, we obtain drag coefficients which are slightly below the solid drag curve. However it is too early to conclude at this stage of the study and further developments are needed. The increase of drag with the shear is also visible for larger bubbles $Re > 100; 6 \leq Sr^{-1} < 10$, but may also include in that case the effect of a slight coupling.

We have compared the present data to results obtained by other authors. Figure (11) presents such a comparison. The more interesting point is that the present data (+) and

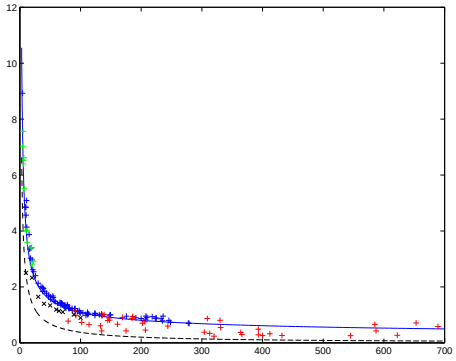

Figure 11: Drag coefficient C_D as a function of Reynolds number Re. + are data from the present study, + are Van Nierop (2003) results for experiments in water, + are Van Nierop *et al.* (2007) results for experiments in water/glycerin mixtures, with $Re > 5$ and x are Naciri (1992) results obtained with water/glycerin mixtures. The plain line is the drag curve for solid spheres and the dashed line is that of clean bubbles

the glycerin/water data of Van Nierop *et al.* (2007) (+) seem to collapse onto a same curve. The data obtained in water by Van Nierop (2003) (+) and the data obtained by Naciri (1992) (x) have drag coefficients that are slightly lower. It is not evident to understand the origin of these differences. Nevertheless, it can be mentioned at this stage that Naciri (1992) worked with larger bubbles than those presented in the other studies. Indeed his bubbles had typical sizes of a few millimeters, which could explain that they are less sensitive to contamination. Van Nierop (2003) have some dispersion in the values of the drag coefficient for bubbles in water. Hence it is difficult to perform a comparison with the present data for example as a function of the Strouhal number because of this dispersion.

4.2 Lift force

On figure (12) lift coefficients are plotted versus the Reynolds number. As for the drag force, the points for $Re \gtrsim 60$ and

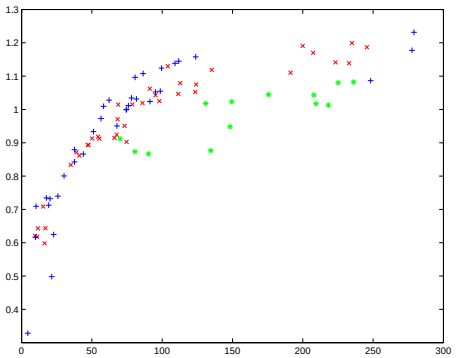

Figure 12: Lift coefficient C_L as a function of Reynolds number Re. + are bubbles with $10 \leq Sr^{-1}$, x are bubbles with $6 \leq Sr^{-1} < 10$, * are bubbles with $4 \leq Sr^{-1} < 6$.

$4 \leq Sr^{-1} < 6$ correspond to a situation where the two-way coupling is significant and must not be considered as representative of the lift force in a pure solid body rotation. Here again we note that the coupling between the bubble and the reference flow tends to diminish the lift coefficient, this effect increasing as the bubble gets closer to the axis of rotation of the flow. In the range $10 \leq Sr^{-1}$ no coupling occurs and lift coefficients collapse onto a single curve. This curve increases first rapidly with Re and then seems to reach an asymptotic level for $Re > 100$. This point still needs to be confirmed by additional measurements in the range $100 < Re < 300$. However, the global trend suggests an asymptotic value of the order of unity which is higher than the 0.5 value predicted by Auton (1987)'potential theory. The reason for this difference remains unclear, but it must be kept in mind that this theory is valid for linear shear flow. Interestingly, the small bubbles ($Re \lesssim 60$) have their lift coefficients on the same curve whatever the value of the dimensionless shear number Sr, thus indicating that the lift essentially depends on the Reynolds number over that range. On the opposite for larger bubbles ($Re > 60 - 70$) in the range ($6 \leq Sr^{-1} < 10$) and where coupling effects remain negligible, we see that an increase of the shear makes the lift coefficient slightly diminish. A more detailed analysis of the data is planned for the future.

We have compared our results with the values of the lift coefficients found in the literature for the same range of flow parameters (see figure (13)). We have not retained for this comparison the study of Sridhar & Katz (1995) which concerns microscopic bubbles entrained by a vortex.

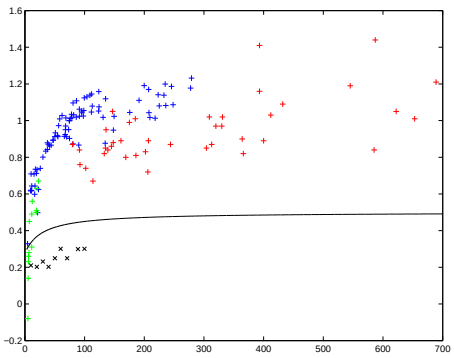

Figure 13: Lift coefficient C_L as a function of Reynolds number Re. + are data from the present study, + are Van Nierop *et al.* (2007) results for experiments in water, + are Van Nierop *et al.* (2007) results for experiments in water/glycerin mixtures, with $Re > 5$ and x are Naciri (1992) results obtained with water/glycerin mixtures. The plain line is the curve obtained by Legendre & Magnaudet (1998).

For $Re > 5$ and $Sr \leq 0.2$, Legendre & Magnaudet (1998) established numerically the following empirical correlation:

$$C_L(Re) = 0.5 \times \frac{1 + 16Re^{-1}}{1 + 29Re^{-1}} \qquad (9)$$

The range of applicability of this equation corresponds to the one of the present data. Legendre & Magnaudet (1998)'s curve also tends toward 0.5 at high Reynolds number. Logically it does not fit our data. The comparison with Van Nierop *et al.* (2007) results gives interesting features. The present "low" Reynolds values of the lift coefficient well coincide with the values obtained by these authors (green plus) and prolong their tendency in the intermediate range of Reynolds number $20 < Re < 70$. This is all the most interesting that the fluid is different in the two studies. Indeed Van Nierop *et al.* (2007) used glycerin for this range of Reynolds number. The comparison with the values at higher Reynolds numbers gives rise to more questions. We see on the figure that there is a discrepancy between the values of the lift coefficient obtained by Van Nierop *et al.* (2007) in water and the present ones. No definitive explanation for the moment can be given. Referring to Van Nierop (2003) this discrepancy could originate from a problem of alignment mentioned by this author in his experiments with water, which seems plausible given the importance of alignment for the determination of the lift coefficient. Despite their data are subject to more dispersion than ours for this reason, it is worth noting that they globally tend to a value which is also higher than 0.5 at high Reynolds number. The other comparison that can be done is with the results of Naciri (1992). Here again the values does not agree with the present values nor with the ones of Van Nierop *et al.* (2007). Although it is difficult to conclude, a possible reason for these discrepancy could be that Naciri (1992) used larger bubbles (eg) bubbles of a few millimeters and that the behavior of such deforming bubbles is different.

5 Oscillations of the bubble

As mentioned before, the bubble never stabilizes on its equilibrium position. but it oscillates around it. The amplitude of the movements are of the order of a few tenths of a millimeter. A primary study shows qualitatively that different sources of oscillation are competing. Three kinds of frequencies are generally obtained, one related with the rotation rate of the tank, and sometimes its harmonics, one associated with a three-dimensional motion of the bubble and sometimes one related with an interaction between the vortex shedding and the bubble. An example of the fourier transform of the x position of the bubble is presented on figure (14). Indeed, when

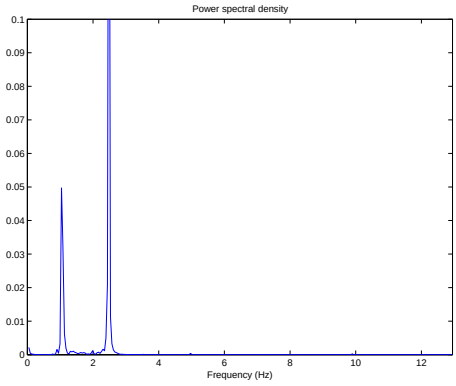

Figure 14: Spectrum of the x-position of a bubble. The rotation rate of the tank was 2.5 turn per second. The first peak corresponds to the three-dimensional motion, the other one to the rotation rate of the tank.

the experiment begins a first phase corresponds to the bubble

coming to its equilibrium position. After this first phase, the bubble appears to be moving around its equilibrium position. During a first laps of time it moves with short movements (few tenths of a millimeter) in the plane in which it stabilized. In the spectrum the rotation rate of the tank and its harmonics are very present. When waiting more, the bubble begins to oscillate also in the third direction (parallel to the axis of rotation) and another peak (around a few hertz) appears while the previous ones can sometimes diminish. For certain kind of bubbles (mean-size bubbles far from the axis of rotation) also appears a frequency around 10 Hz. This frequency is of the order of magnitude of the frequency at which vortices are released from the bubble. It seems reasonable to believe that the presence of this frequency in the spectrum could be linked to an interaction between the vortex shedding and the bubble trajectory. In future work, we intend to investigate these phenomena and try to give a full explanation of the sources of excitement of the bubble and how it reacts to them. For what concerns the lift and drag coefficients it should be mentioned that whatever the "regime" of frequency in which the measurement is performed the equilibrium position is the same and so does the value of the forces.

6 Conclusion

The behavior of a single bubble included in a solid body rotation flow has been studied. The equilibrium position of the bubble has been measured for moderate to high Reynolds number, low to moderate dimensionless shear number Sr, and the drag and lift coefficients calculated from this position. To have reliable results an important effort was done to characterize the reference flow. Using PIV, the flow has been checked to have a linear velocity profile on the whole section of the tank. The small movements of the axis of rotation of the flow have also been studied and quantified. Because they are small, these movements appear as having no influence for the determination of the lift and drag coefficients. On the other hand the rotation rate of the tank appears in the frequencies of these movements and can be a source of excitation for the bubble. The possible coupling of the bubble, its wake and the solid rotating flow have been also investigated in detail with PIV. For $Re \lesssim 60 - 70$, the flow arriving on the bubble is not modified whatever the position of the bubble close to the axis of rotation and thus the Strouhal number Sr. This seems due to the fact that the wake is very thin in that case. For larger Reynolds numbers ($Re \gtrsim 100$), a significant coupling occurs when $Sr^{-1} \lesssim 6$ and this perturbs the flow arriving on the bubbles. For $6 \lesssim Sr^{-1} \lesssim 10$, the coupling is weak so that it does not influence significantly the incident flow on the bubbles and for $10 \lesssim Sr^{-1}$ no perturbation is felt back by the bubble. The drag and lift coefficients obtained over the range of parameter where the incident flow on the bubble is not perturbed and can be considered as a pure solid body rotation exhibits interesting trends. Concerning the drag, the coefficients obtained are closed to the ones of solid spheres, probably because of a partial contamination of interfaces and increases significantly with the shear. This agrees with results found by Van Nierop *et al.* (2007). The lift force coefficients come in continuity with the values obtained in glycerin by Van Nierop *et al.* (2007) at low Reynolds number and tend asymptotically to a value of order unity which is higher than the 0.5 value of Auton (1987)' potential theory for linear shear flow. This qualitatively agree with the measurements in water of Van Nierop *et al.* (2007) which are also higher than 0.5. Interestingly, the lift coefficient seems to be independent of Sr for Reynolds numbers below 60-70 and to slightly decrease with Sr for large bubbles having Reynolds number above 100. Because the bubble never stabilizes on its equilibrium position, its small movements have been studied showing the presence of different frequencies among which one outstanding an interaction of the bubble with its own wake. Future work will come to give explanations to these different points that remain at the moment effective but with a partial explanation.

References

Auton, T.R., The dynamics of bubbles, drops and particles in motion in liquids, Ph.D. dissertation, University of Cambridge (1983)

Auton, T.R., The lift force on a spherical body in a rotational flow. Journal of Fluid Mechanics, Volume 183, 199 – 218 (1987)

Clift, R., Grace, J.R., Weber, M.E., Bubbles, Drops and Particles, Academic (1978)

Lamb, H., Hydrodynamics, 6th edition, Dover (1934)

Legendre, D. & Magnaudet, J., A note on the lift force on a spherical bubble or drop in a low-Reynolds-number shear flow, Physics of Fluids, Volume 9, Number 11, 3572 – 3574 (1997)

Legendre, D. & Magnaudet, J., The lift force on a spherical bubble in a viscous linear shear flow. Journal of Fluid Mechanics, Volume 368, 81 – 126 (1998)

Lu, J., Biswas, S., Tryggvason, G., A DNS study of laminar bubbly flows in a vertical channel. International journal of multiphase flow, Volume 32, Number 6, 643 – 660 (2006)

Magnaudet, J. & Eames, I., Dynamics of high Re bubbles in inhomogeneous flows. Annual Review of Fluid Mechanics, Volume 32, 659 – 708 (2000)

McLaughlin, J.B., Inertial migration of a small sphere in linear shear flows. Journal of Fluid Mechanics, Volume 224, 261 – 274 (1991)

Mei, R., Klausner, J., Lawrence, C., A note on the history force on a spherical bubble at finite Reynolds number. Physics of Fluids, Volume 6, 418–420 (1994)

Naciri, A. Contribution à l'étude des forces exercées par un liquide sur une bulle de gaz: portance, masse ajoutée et interactions hydrodynamiques. Thèse, Ecole Centrale de Lyon (1992)

Sridhar, G. & Katz, J., Drag and lift forces on microscopic bubbles entrained by a vortex. Physics of Fluids, Number 2, Volume 7, 389 – 399 (1995)

Saffman, P.G., The lift force on a small sphere in a slow shear flow. Journal of Fluid Mechanics, Volume 22, 385 – 400 (1965), Corrigendum: Journal of Fluid Mechanics, Volume 31, 624 (1968)

van Nierop, E.A., Towards controlling bubbles - understanding lift, Master's thesis (2003)

van Nierop, E.A., Luther, S., Bluemink, J.J., Magnaudet, J., Prosperetti, A.,Lohse D., Drag and lift forces on bubbles in a rotating flow. Journal of Fluid Mechanics, Volume 571, 439 – 454 (2007)